The Principles of Stroboscopic Detection of Nuclear Forward-Scattered Synchrotron Radiation

R. Callens,[1,*] R. Coussement,[1,2] T. Kawakami,[3] J. Ladrière,[4] S. Nasu,[3]
T. Ono,[3] I. Serdons,[1] K. Vyvey,[1] T. Yamada,[5] Y. Yoda,[5] and J. Odeurs[1]

[1]*Instituut voor Kern- en Stralingsfysica, K.U.Leuven, Celestijnenlaan 200D, B-3001 Leuven, Belgium.*
[2]*Optique Nonlinéaire Théorique, Université Libre de Bruxelles, Campus Plaine CP 231, Bld. du Triomphe, B-1050 Bruxelles, Belgium.*
[3]*Graduate School of Engineering Science, Osaka University, Toyonaka, Osaka 560-8531, Japan.*
[4]*Laboratory of Nuclear Chemistry, Université Catholique de Louvain, Chemin du cyclotron, 1348 Louvain-la-Neuve, Belgium.*
[5] *Japan Synchrotron Radiation Research Institute, Kouto 1-1-1, Mikazuki-cho, Sayo-gun, Hyogo 679-5198, Japan.*

(Dated: June 27, 2002)

The basic principles of stroboscopic detection of nuclear resonant forward-scattered synchrotron radiation are thoroughly discussed. It is explained how the experiment can be configured in such a way that energy-resolved spectra with a straightforward interpretation are obtained. The theory is supported by a set of experimental spectra on the single-line compound potassium ferrocyanide trihydrate. Further, it is shown that a stroboscopic measurement is equivalent to an interferometer experiment. Finally, a comparison of stroboscopic detection and other Mössbauer techniques is given.

PACS numbers: 76.80.+y,41.60.Ap,82.80.Ej

I. INTRODUCTION

The study of hyperfine interactions is important for a better understanding of the magnetic and electric properties in solids. Many techniques were developed for the study of these interactions, of which Mössbauer spectroscopy is best known. In 1974 Ruby[1] suggested to replace the conventional radioactive source by synchrotron radiation. The synchrotron source has the advantage that it provides linearly polarized, well-collimated and intense radiation. Moreover, the energy of the beam is tunable over a wide range. However, the replacement of the radioactive source by the synchrotron source is not straightforward due to the totally different time and energy structure. The synchrotron source produces a periodic set of ultra short pulses (∼100 ps) with a broad energy bandwidth (several orders of magnitude broader than the width of the Mössbauer isomer). Therefore, only a very small fraction of the incident beam interacts with the nuclei. This explains why we had to wait a full decade before delayed nuclear resonant scattered photons could be observed.[2] The first nuclear resonant scattering experiment in the forward direction was reported in 1991.[3] It was shown that the hyperfine interaction parameters can be extracted from the time evolution of the nuclear resonant scattered intensity. During the past decade, this detection scheme has been further exploited and the nuclear forward scattering technique has become one of the standard hyperfine interaction techniques.[4] Alternative detection schemes are the nuclear lighthouse effect[5] and the Synchrotron Mössbauer Source[6]. Recently, first experimental results with a new technique, stroboscopic detection of nuclear resonant scattered synchrotron radiation, have been published.[7] This technique provides energy-resolved spectra and, hence, combines the advantages of conventional Mössbauer spectroscopy and synchrotron radiation. Moreover, the time between two synchrotron bunches is only limited by the time resolution of the detector and the electronics. Therefore, the technique is suitable for the study of long-lived isomers, e.g., ^{181}Ta.

In this article we will further explore the strengths and the limitations of the stroboscopic detection scheme with the aid of new experimental data. Section II qualitatively sketches the mechanism of stroboscopic detection. It is intuitively shown how the restriction of the data acquisition to a periodic set of time windows gives rise to stroboscopic resonances. In section III the full mathematical description of these stroboscopic resonances is given. It is shown that the spectrum is built up of different order stroboscopic spectra, each resembling a conventional Mössbauer spectrum. Also a simulation of the spectrum of α-iron with a randomly hyperfine field is discussed. Sections IV and V contain the experimental details and experimental spectra of single-line samples. With the help of these spectra the influence of the frequency and the symmetry of the time window is discussed. An important aspect of stroboscopic detection is the absence of the radiative coupling[8] at velocities corresponding to the higher order stroboscopic resonances. Therefore, a stroboscopic measurement is equivalent to an interferometer experiment. This is discussed in detail in section VI. Finally, a comparison of stroboscopic detection and other Mössbauer techniques is given in section VII.

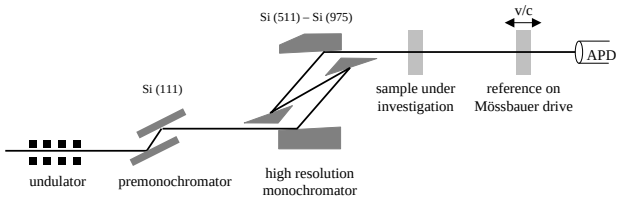

FIG. 1: Experimental setup.

II. QUALITATIVE APPROACH

Stroboscopic measurements are performed in the heterodyne detection scheme,[9,10] relying on the comparison of the unknown transition frequencies in the sample under investigation with a variable reference frequency. Therefore, a second single-line reference sample is included in the conventional nuclear forward scattering experimental setup (Fig. 1). By mounting this sample on a Mössbauer drive, the resonance frequency can be varied by hundreds of units of the natural line width. In the heterodyne scheme three scattering paths can be distinguished: scattering in the sample under investigation, scattering in the reference sample and scattering in both samples (the radiative coupling between both samples).[8] Because of the large coherence length of the synchrotron photon, these paths are coherent and, hence, can interfere. The broadband character of the photon allows the coherent excitation of the energy levels within this bandwidth, resulting in quantum beats in the time spectrum. It is instructive to consider two single-line absorbers with resonance energies $\hbar\omega_1$ and $\hbar\omega_r$, respectively. In this case, only one quantum beat will be observed. At zero velocity its frequency equals $|\omega_r - \omega_1|$. By varying the Doppler velocity of the reference sample, the reference frequency, ω_r, is modulated by the Doppler shift $\Delta = \omega_r(v/c)$. Therefore, the quantum beat frequency changes to $|\omega_r + \Delta - \omega_1|$. If the time-integrated intensity is measured, the quantum beat will level out. Only if the Doppler shift is such that the quantum-beat period is of the order of or larger than the lifetime τ of the Mössbauer isomer, a non-vanishing contribution of the quantum beat remains after time integration. This condition is fulfilled if $\Delta \approx \omega_1 - \omega_r$. At the corresponding Doppler velocity a resonance will be observed. Therefore, a time-integrated spectrum as a function of the Doppler velocity of the reference sample is very similar to a Mössbauer spectrum obtained with a radioactive source. However, full time integration is only possible if the prompt non-scattered radiation is reduced by extra devices, e.g., a polarizer and analyzer.[11]

The way followed in this paper to eliminate the prompt radiation is stroboscopic data acquisition. This means that the data acquisition is restricted to a periodic set of time windows. If the timing is tuned in such a way that no data are recorded during the arrival time of the prompt synchrotron pulses, all data result from photons

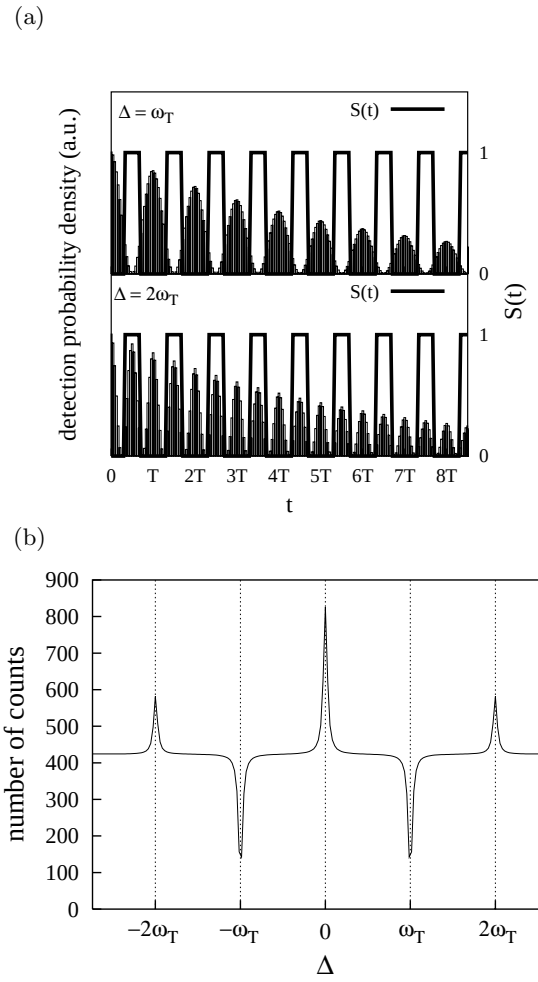

FIG. 2: Simulated spectra in the case of two identical thin single-line samples (a) Simulated detection probability as a function of the scattering time at different stroboscopic resonance conditions ($\Delta = n\omega_T = n\ 2\pi/T$, $n = 1, 2$). The set of time windows ($S(t)$) is indicated by the solid line. (b) Intensity accumulated in the set of time windows shown in figure (a) as a function of the Doppler shift Δ.

that are delayed due to the nuclear interaction with the samples. The use of time windows induces extra resonances at velocities for which the quantum beat frequency equals a multiple of the time-window frequency ($|\omega_r + \Delta - \omega_1| = n\omega_T$, with n an integer describing the stroboscopic order and ω_T the time-window frequency). This is illustrated in Fig. 2. This figure contains simulated spectra for two identical thin single-line absorbers. Note that in this case $\omega_1 = \omega_r$ and, therefore, the resonance condition reduces to $\Delta = n\omega_T$. Fig. 2(a) shows the time evolution of the probability density to detect a photon that was generated at time 0 and was delayed by a time t due to scattering by the absorbers. The corresponding Doppler shift is chosen so that the resonance condition $\Delta = \omega_T$ ($n = 1$) or $\Delta = 2\omega_T$ ($n = 2$) is fulfilled. The chosen set of time windows, which is indicated by the solid line, selects a minimum in the intensity for

$n = 1$ and a maximum for $n = 2$, respectively. Consequently, a negative resonance appears at $\Delta = \omega_T$ and a positive resonance at $\Delta = 2\omega_T$ in the stroboscopic spectrum as function of the Doppler shift (Fig. 2(b)). For samples with hyperfine split energy levels, each stroboscopic resonance is replaced by a series of resonances, each one resembling a Mössbauer spectrum with a conventional source, as will be further explained in the next section (Fig 4).

III. QUANTITATIVE APPROACH

The previous section demonstrates qualitatively the origin of the stroboscopic resonances. However, in order to develop a simulation and evaluation program, the stroboscopic concept should be accompanied by a mathematical theory. This theory is described in this section. In subsection A it will be shown that the total spectrum can be decomposed in several components $d_n(\Delta)$ with a weighting factor s_n. The partial spectra $d_n(\Delta)$ only depend on the properties of the samples while the factors s_n are fully determined by the set of time windows. Subsection B and C deal with these spectra $d_n(\Delta)$ and the coefficients s_n, respectively. Finally, in subsection D the full spectrum is discussed in detail. It will be mathematically shown how the frequency of the set of time windows influences the shift of the stroboscopic resonances, while the symmetry of the set of time windows affects the shape of the resonances.

A. Derivation of the general formula

A stroboscopic spectrum contains the number of photons that are detected in a certain set of time windows as a function of the Doppler velocity of the reference absorber. We will express the intensity as a function of the Doppler shift, Δ, of the reference frequency, which is proportional to the Doppler velocity

$$\Delta = \omega_r(v/c). \tag{1}$$

Because there is no coherence between photons generated by different electron bunches, the probability to detect a photon as a function of time is the sum of the probabilities corresponding to the different bunches. The contribution of each bunch is equal if the set of time windows stays unaffected after shifting over a bunch period. This condition is fulfilled if the time-window frequency equals a multiple of the bunch frequency ($\omega_T = m\omega_B$, with ω_T the time-window frequency and ω_B the bunch frequency). Therefore, in the following we will restrict the calculation to the contribution of one bunch.

The detection probability within the set of time windows is given by

$$I_S(\Delta) = \int_0^{+\infty} dt\ S(t)D(t,\Delta) \tag{2}$$

with $D(t,\Delta)$ the probability density for detecting a photon with scattering time t and $S(t)$ the time-window function. This time-window function equals 1 within the data acquisition intervals and 0 elsewhere. $S(t)$ is periodic with a frequency ω_T. Therefore, $S(t)$ can be expanded in a Fourier series and we obtain

$$\begin{aligned} I_S(\Delta) &= \int_0^{+\infty} dt \sum_{n=-\infty}^{+\infty} s_n \exp(in\omega_T t) D(t,\Delta) \\ &= \sum_{n=-\infty}^{+\infty} s_n \int_0^{+\infty} dt\ D(t,\Delta)\exp(in\omega_T t) \end{aligned}$$

with

$$s_n = \frac{1}{T}\int_0^T dt\ S(t)\exp(-in\omega_T t). \tag{3}$$

If we define

$$d_n(\Delta) = \int_0^{+\infty} dt\ D(t,\Delta)\exp(in\omega_T t), \tag{4}$$

$I_S(\Delta)$ can be written as

$$I_S(\Delta) = \sum_{n=-\infty}^{+\infty} s_n d_n(\Delta). \tag{5}$$

Equation 5 shows that the spectrum is built up of different components $d_n(\Delta)$ with weighting factors s_n. We will now further derive the shape of the spectra, $d_n(\Delta)$, and discuss how the weighting factors, s_n, depend on the chosen set of time windows.

B. The spectrum components $d_n(\Delta)$

In order to discuss the spectrum components, $d_n(\Delta)$, a more explicit formula should be derived. This can be done by expressing the detection probability density $D(t,\Delta)$ in Eq. 4 in terms of the scattering amplitude $\vec{A}(t,\Delta)$

$$D(t,\Delta) = |\vec{A}(t,\Delta)|^2 = \vec{A}(t,\Delta)\cdot\vec{A}(t,\Delta). \tag{6}$$

Generally, the scattering amplitude $\vec{A}$ is given by a complex two-component vector taking into account the two polarization components. The dot product used above is defined as

$$\vec{A}_1\cdot\vec{A}_2 = A_{1,x}A^*_{2,x} + A_{1,y}A^*_{2,y} \tag{7}$$

with $A_{1,x}$, $A_{2,x}$, $A_{1,y}$, and $A_{2,y}$ the vector components in the basis of linear polarization or

$$\vec{A}_1\cdot\vec{A}_2 = A_{1,+}A^*_{2,+} + A_{1,-}A^*_{2,-} \tag{8}$$

with $A_{1,+}$, $A_{2,+}$, $A_{1,-}$, and $A_{2,-}$ the vector components in the basis of circular polarization. Using the Fourier expansion of the amplitude $\vec{A}(t,\Delta)$

$$\vec{A}(t,\Delta) = \frac{1}{2\pi}\int_{-\infty}^{+\infty} d\omega\ \vec{A}(\omega,\Delta)\exp(i\omega t)$$

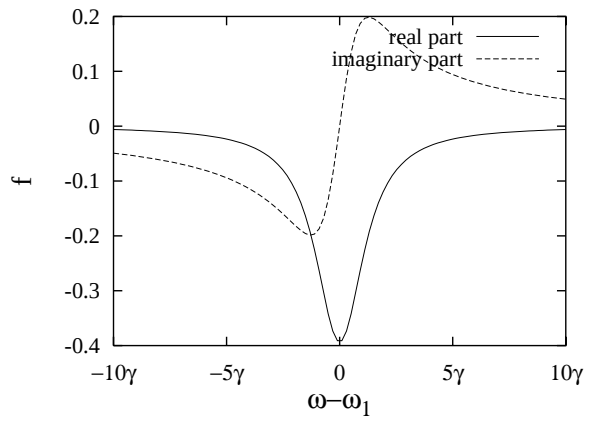

FIG. 3: The real and imaginary part of the forward scattering factor $f(\omega-\omega_1)$ in the vicinity of the resonance energy for a single-line absorber with effective thickness $L=1$.

we obtain for $d_n(\Delta)$

$$d_n(\Delta)=\frac{1}{2\pi}\int_{-\infty}^{+\infty} d\omega\ \vec{A}(\omega,\Delta)\cdot\vec{A}(\omega+n\omega_T,\Delta). \quad (9)$$

$d_n(\Delta)$ is the dot product of the scattering amplitude and the amplitude shifted over $-n\omega_T$, integrated over all frequencies. This general formula is the basis of our simulation and evaluation program.

From Eq. 9 it is clear that $d_n(\Delta)$ is fully determined by the amplitude $\vec{A}(\omega,\Delta)$. In the stroboscopic detection scheme, $\vec{A}(\omega,\Delta)$ is the amplitude of a photon that is scattered by two absorbers. Hence, it can be written as a sum of three amplitudes: $\vec{A}_s$, describing nuclear resonant scattering in the sample under investigation, $\vec{A}_r$, describing nuclear resonant scattering in the reference sample and $\vec{A}_{s,r}$, describing the scattering by both samples (the radiative coupling between both samples).[8] In frequency domain, the scattering amplitude is proportional to the amplitude $\vec{A}_{in}$ of the incident photon and, hence, $\vec{A}(\omega,\Delta)$ can be expressed as

$$\begin{aligned}\vec{A}(\omega,\Delta) &= \vec{A}_s+\vec{A}_r+\vec{A}_{s,r}\\ &= \big(f_s(\omega-\omega_i)+f_r(\omega-\omega_r-\Delta)\\ &\quad +f_s(\omega-\omega_i)f_r(\omega-\omega_r-\Delta)\big)\vec{A}_{in}\ . \quad (10)\end{aligned}$$

Since the spectral bandwidth of the synchrotron radiation is very large with respect to the widths involved in the resonant scattering matrices, $\vec{A}_{in}$ can be considered as frequency-independent. Generally, the nuclear resonant scattering matrix f is polarization dependent and given by a 2 by 2 complex matrix.[10] The matrix f can be approximated by 0, except in the vicinity of the resonance frequencies ω_i and $\omega_r+\Delta$ for the sample under investigation and the reference sample, respectively.

In the case of a single-line sample with resonance energy $\hbar\omega_1$, the scattering matrix f can be replaced by a scalar scattering factor[8]

$$f(\omega-\omega_1)=\exp(iL\frac{\gamma/4}{\omega-\omega_1-i\gamma/2})-1. \quad (11)$$

Here, we introduced the effective thickness $L=\sigma_0 f_{LM} n d$, where σ_0 is the maximum resonance cross section, f_{LM} the Lamb-Mössbauer factor, n the density of resonant nuclei and d the sample thickness. γ is the inverse of the Mössbauer lifetime. The real and imaginary parts of this amplitude for $L=1$ are displayed in Fig. 3. For thin samples ($L\ll 1$) Eq. 11 can be approximated by

$$f(\omega-\omega_1)=iL\frac{\gamma/4}{\omega-\omega_1-i\gamma/2}. \quad (12)$$

Note that in the above description only nuclear resonant scattering was considered. The electronic scattering factor is frequency-independent and, hence, does not depend on the Doppler shift, Δ, of the reference frequency. Electronic scattering gives rise to an overall reduction of the intensity only and, therefore, this factor can be omitted without loss of generality and reintroduced when appropriate.

Returning to Eq. 9, the spectrum components $d_n(\Delta)$ can now be decomposed in several terms by replacing the scattering amplitude by Eq. 10

$$d_n(\Delta)=\alpha_n(\Delta)+\alpha^*_{-n}(\Delta)+\beta_{s,n}+\beta_{r,n}+\rho_n(\Delta). \quad (13)$$

$\alpha_n(\Delta)$ and $\alpha^*_{-n}(\Delta)$ are defined by

$$\alpha_n(\Delta) = \frac{1}{2\pi}\int_{-\infty}^{+\infty} d\omega\ [f_s(\omega-\omega_i)\vec{A}_{in}]\cdot[f_r(\omega-\omega_r-\Delta+n\omega_T)\vec{A}_{in}] \quad (14)$$

$$\alpha^*_{-n}(\Delta) = \frac{1}{2\pi}\int_{-\infty}^{+\infty} d\omega\ [f_r(\omega-\omega_r-\Delta)\vec{A}_{in}]\cdot[f_s(\omega-\omega_i+n\omega_T)\vec{A}_{in}]. \quad (15)$$

These terms describe the interference between scattering in the sample under investigation and scattering in the

reference sample. Therefore, we will call these terms the pure interference terms. Note that $\alpha_n(\Delta)$ only differs from 0 if $\Delta \approx \Omega_{n,i}$ with $\Omega_{n,i} = \omega_i - \omega_r + n\omega_T$ and, hence, it describes resonances that are shifted by $n\omega_T$ from the position $\Delta = \omega_i - \omega_r$. Remark also that only the overall shift of the resonances is determined by the set of time windows. The relative position determined by the hyperfine interactions and the width of the resonances in $\alpha_n(\Delta)$ is fully determined by the characteristics of the samples. In order to determine the shape of the resonances, we will take the example of two thin single-line absorbers. In this case, the scattering matrices $f_{s,r}$ can be replaced by scalar scattering factors given in Eq. 12 resulting in

$$\begin{aligned}\alpha_n(\Delta) &= L_s L_r \frac{\gamma^2}{16}|\vec{A}_{in}|^2 \frac{1}{2\pi}\int_{-\infty}^{+\infty} d\omega \; \frac{1}{(\omega-\omega_1-i\gamma/2)(\omega-\omega_r-\Delta+n\omega_T+i\gamma/2)} \\ &= L_s L_r \frac{\gamma^2}{16}|\vec{A}_{in}|^2 \frac{\gamma + i(\Omega_{n,1}-\Delta)}{(\Omega_{n,1}-\Delta)^2+\gamma^2}, \end{aligned} \tag{16}$$

where $\Omega_{n,1} = \omega_1 - \omega_r + n\omega_T$ defines the position of the resonances. From Eq. (16) it follows that the real part of $\alpha_n(\Delta)$ is lorentzian while the imaginary part is dispersive.

The terms $\beta_{s,n}$ and $\beta_{r,n}$ of Eq. 13 are given by

$$\beta_{s,n} = \frac{1}{2\pi}\int_{-\infty}^{+\infty} d\omega \; [f_s(\omega-\omega_i)\vec{A}_{in}]\cdot[f_s(\omega-\omega_i+n\omega_T)\vec{A}_{in}] \tag{17}$$

$$\beta_{r,n} = \frac{1}{2\pi}\int_{-\infty}^{+\infty} d\omega \; [f_r(\omega-\omega_r)\vec{A}_{in}]\cdot[f_r(\omega-\omega_r+n\omega_T)\vec{A}_{in}]. \tag{18}$$

These terms describe the scattering in the sample under investigation and the scattering in the reference sample, respectively. These terms are independent of the Doppler shift, Δ, and, hence, contribute to the baseline.

$\rho_n(\Delta)$ collects the terms in which the radiative coupling part of the amplitude (last term of Eq. 10) is involved and is explicitly given by

$$\rho_n(\Delta) = \rho_{s,n}(\Delta) + \rho^*_{s,-n}(\Delta) + \rho_{r,n}(\Delta) + \rho^*_{r,-n}(\Delta) + \rho_{s,r,n}(\Delta) \tag{19}$$

with

$$\rho_{s,n}(\Delta) = \frac{1}{2\pi}\int_{-\infty}^{+\infty} d\omega \; [f_s(\omega-\omega_i)\vec{A}_{in}]\cdot[f_s(\omega-\omega_i+n\omega_T)f_r(\omega-\omega_r-\Delta+n\omega_T)\vec{A}_{in}] \tag{20}$$

$$\rho_{r,n}(\Delta) = \frac{1}{2\pi}\int_{-\infty}^{+\infty} d\omega \; [f_r(\omega-\omega_r-\Delta)\vec{A}_{in}]\cdot[f_s(\omega-\omega_i+n\omega_T)f_r(\omega-\omega_r-\Delta+n\omega_T)\vec{A}_{in}] \tag{21}$$

$$\rho_{s,r,n}(\Delta) = \frac{1}{2\pi}\int_{-\infty}^{+\infty} d\omega \; [f_s(\omega-\omega_i)f_r(\omega-\omega_r-\Delta)\vec{A}_{in}]\cdot[f_s(\omega-\omega_i+n\omega_T)f_r(\omega-\omega_r-\Delta+n\omega_T)\vec{A}_{in}]. \tag{22}$$

The larger the effective thickness of the samples, the larger the contribution of these terms. Smirnov[8] has shown that the sign of the radiative coupling terms $\rho_n(\Delta)$ is opposite to the sign of the pure interference terms $\alpha_n(\Delta) + \alpha^*_{-n}(\Delta)$. Hence, the radiative coupling generally decreases the signal-to-baseline ratio. This will be extremely important for thick absorbers.

In the special case $n = 0$ we find that $d_0(\Delta)$ is the heterodyne spectrum[9,10] or the spectrum we would have obtained if there were overall time integration ($S(t) = 1$ for all t). For $n \neq 0$ an interesting case arises if $n\omega_T$ is larger than the range of the transition frequencies. Because the scattering matrix $f_s(\omega-\omega_i)$ can be approximated by 0 outside this frequency range, either the scattering matrix $f_s(\omega-\omega_i)$ or the shifted scattering matrix $f_s(\omega-\omega_i+n\omega_T)$ approximates 0 for all values of ω. The same holds for the scattering matrix $f_r(\omega-\omega_r-\Delta)$ and the shifted scattering matrix $f_r(\omega-\omega_r-\Delta+n\omega_T)$. Consequently, at this condition the baseline terms $\beta_{s,n}$ and $\beta_{r,n}$ and the radiative coupling term $\rho_n(\Delta)$ vanish. Hence, only the two pure interference terms remain

$$d_n(\Delta) = \alpha_n(\Delta) + \alpha^*_{-n}(\Delta). \tag{23}$$

C. The weighting factors, s_n, for a square time window

According to Eq. 5 each spectrum component $d_n(\Delta)$ is present in the final spectrum with a weighting factor s_n that only depends on the chosen set of time windows. Note that the relation $s_{-n} = s^*_n$ holds because the set of time windows is described by a real function $S(t)$. Therefore, in the calculation of s_n we can restrict to $n \geq 0$. For

a function $S'(t)$ symmetric around $t = 0$, with $t = 0$ defined as the arrival time of the prompt synchrotron radiation pulse, the imaginary part of the Fourier coefficients s'_n vanishes (integration of an odd function), resulting in

$$s'_n = \frac{1}{T}\int_T dt\ S'(t)\cos(n\omega_T t). \tag{24}$$

If the function $S'(t)$ is shifted along the time axis, an additional phase factor is introduced. Therefore, the Fourier coefficients of the shifted time-window function $S(t)$ symmetric around $t_0 \neq 0$ are given by

$$s_n = \exp(-in\omega_T t_0)\ s'_n. \tag{25}$$

Note that for a time window that is symmetric around $t_0 = T/2$, the phase factor reduces to $(-1)^n$ resulting in real s_n. In the specific case of a square time window we get

$$s_n = \exp(-in\omega_T t_0)\frac{\sin(n\pi F)}{n\pi}. \tag{26}$$

with F the allowed fraction or the fraction of the time-window period for which $S(t) = 1$. From Eq. 26 we learn that $|s_n|$ is determined by the allowed fraction F while the phase is related to the center of the time window, t_0.

D. The total spectrum $I_S(\Delta)$.

The above subsections provide all the ingredients necessary to discuss the total spectrum. In a first stage, the description of the total spectrum will be restricted to ω_T larger than the range of the resonance frequencies in the sample. In this case, the spectrum components $d_n(\Delta)$ can be approximated by Eq. 23 for $n \neq 0$. Hence, Eq. 5 can be simplified

$$I_S(\Delta) = I^0(\Delta) + \sum_{n\neq 0} s_n(\alpha_n(\Delta) + \alpha^*_{-n}(\Delta)) \tag{27}$$

with $I^0(\Delta)$ the zeroth-order spectrum given by

$$\begin{aligned} I^0(\Delta) &= s_0 d_0(\Delta) \\ &= s_0(\alpha_0(\Delta) + \alpha^*_0(\Delta) + \beta_{s,0} + \beta_{r,0} + \rho_0(\Delta)). \end{aligned} \tag{28}$$

Remember that $d_0(\Delta)$ describes the heterodyne spectrum or the spectrum we would obtain without time-gating. Therefore, $I^0(\Delta)$ is the heterodyne spectrum scaled with the real factor

$$s_0 = \frac{1}{T}\int_T dt\ S(t).$$

Note that, in contrary to the results of Tischler et al.,[12] the width of the resonances in $I^0(\Delta)$ does not depend on the selected set of time windows. This can intuitively be understood by noticing that Tischler et al. selected only one time window within one lifetime, while in stroboscopic detection a set of time windows is selected. Consequently, both data corresponding to short scattering times as data corresponding to long scattering times contribute to the spectrum.

Expression 27 for $I_S(\Delta)$ can further be simplified using the relation $s_n = s^*_{-n}$:

$$\begin{aligned} I_S(\Delta) &= I^0(\Delta) + \sum_{n\neq 0}[s_n\alpha_n(\Delta) + (s_{-n}\alpha_{-n}(\Delta))^*] \\ &= I^0(\Delta) + \sum_{n\neq 0} I^n_{int}(\Delta) \end{aligned} \tag{29}$$

with

$$I^n_{int}(\Delta) = 2\Re(s_n\alpha_n(\Delta)). \tag{30}$$

The spectrum component $I^n_{int}(\Delta)$ is fully determined by the Fourier coefficient s_n given by Eq. 3 and the pure interference term $\alpha_n(\Delta)$ given by Eq. 14. It describes resonances at the positions $\Delta = \Omega_{n,i}$ with $\Omega_{n,i} = \omega_i - \omega_r + n\omega_T$. This is the resonance condition of paragraph II, generalized for samples with hyperfine split energy levels. Therefore, we can identify $I^n_{int}(\Delta)$ with the stroboscopic resonances of order n. Subsequent stroboscopic order resonances have a relative shift of $\Omega_{n+1,i} - \Omega_{n,i} = \omega_T$. Therefore, by choosing the time-window frequency, ω_T, larger than the resonance frequency range in the sample, the different stroboscopic order resonances do not overlap. Hence, $I^n_{int}(\Delta)$ is only superposed on the baseline of the zeroth-order spectrum $s_0(\beta_{s,0} + \beta_{r,0})$. Note that the relative position of the resonances within one stroboscopic order spectrum equals the relative position of the resonance frequencies ω_i. Hence, the interpretation of $I^n_{int}(\Delta)$ in terms of the hyperfine parameters is similar as in a conventional Mössbauer spectrum. The shape of the resonances is determined by the phase of the coefficients s_n, which only depends on the symmetry of the set of time windows. Generally, s_n is a complex number and the resonances are a superposition of a lorentzian-like (the real part of $\alpha_n(\Delta)$) and dispersion-like (the imaginary part of $\alpha_n(\Delta)$) curves with a weighting factor $\Re(s_n)$ and $-\Im(s_n)$, respectively. However, the time window can be chosen symmetrically around $t_0 = T/2$ so that s_n is real, resulting in lorentzian-like resonances. This is illustrated by the simulated spectrum for an α-Fe foil with randomly oriented hyperfine field ($L = 30$) and a stainless steel reference foil ($L = 5$) (Fig. 4). For this simulation a set of time windows with a frequency $\omega_T = 352.2 \times 10^6$ Hz (which corresponds to a period $T = 2.84$ ns) and an allowed fraction $F = 0.5$ (which corresponds to a time window from 0.71 ns till 2.13 ns) was chosen. The different stroboscopic order spectra can be nicely distinguished and the interpretation of the spectra in terms of hyperfine parameters is similar to the interpretation of a Mössbauer spectrum with a radioactive source.

Until now, we restricted to ω_T larger than the frequency range in the sample, resulting in well-separated

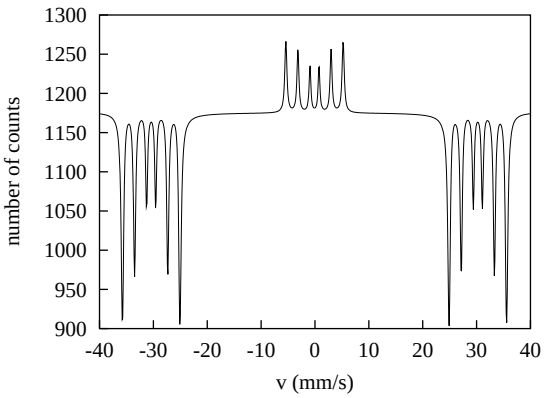

FIG. 4: Simulated spectrum for α-Fe ($L = 30$) with a randomly oriented hyperfine field and a stainless steel reference foil ($L = 5$). The chosen set of time windows has a period of 2.84 ns and lasts from 0.71 ns till 2.13 ns.

stroboscopic order spectra. However, in a real experiment, the time-window frequency is limited by the time-resolution of the detectors and the electronics and this severe condition cannot always be fulfilled. If the time-window frequency is smaller than the frequency range in the sample, different stroboscopic order resonances will overlap and the radiative coupling can no longer be neglected for small $n > 1$. Nevertheless, our simulation and evaluation program can still handle this case as it is based on the general Eq. 9. In an earlier article[7] we described an experiment in which the different stroboscopic order spectra slightly overlap. The spectra could still be analyzed and the hyperfine parameters extracted.

IV. EXPERIMENTAL DETAILS

An experiment that demonstrates the feasibility of the concept was performed at the Nuclear Resonant Scattering beamline BL09[13] at SPring-8. For both samples we used potassium ferrocyanide trihydrate[14] ($K_4Fe(CN)_6.3H_20$) as single-line compound. Hence, the resonance energies in both samples coincide ($\omega_1 = \omega_r$). The resonance energy of the Mössbauer transition in ^{57}Fe is 14.4 keV, which corresponds to a resonance frequency of $\omega_1 = \omega_r = 14.4$ keV$/\hbar = 2.19 \times 10^{19}$ Hz. A bunch mode with a bunch interval $T_B = 23.6$ ns or a bunch frequency $\omega_B = 2\pi/23.6$ ns $= 2.66 \times 10^8$ Hz was used. The photons were detected by an Avalanche Photo Diode (APD) detector with a diameter of 1 mm and a depletion depth of 10 μm. This detector has an efficiency of about 1%. Figure 5 gives the time response of the detector and electronics to the prompt pulse. Although the width at FWHM is about 0.3 ns, the response function has a long tail. In our experiment the bandwidth of the synchrotron pulse was about 10^6 times larger than the bandwidth of the nuclear resonances. Hence, in order to make sure the detected photons were delayed, the response to the

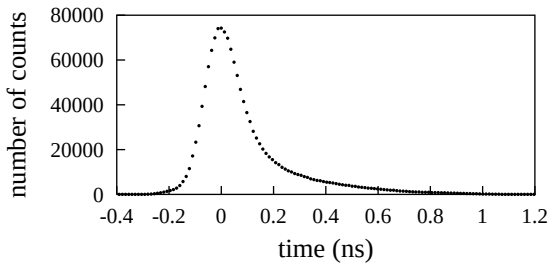

FIG. 5: Time response of the detector to the prompt pulse.

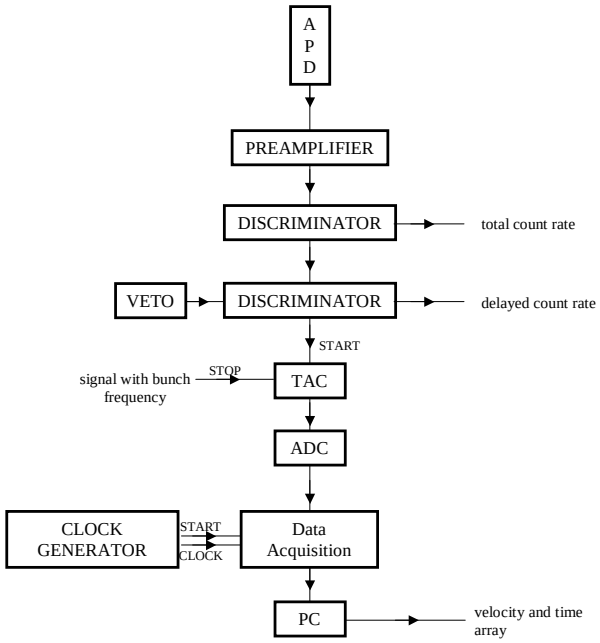

FIG. 6: Scheme of the data acquisition.

prompt pulse should be reduced by a factor 10^6. This explains why in the measurements described below we put a veto window of about 5 ns centered around the arrival time of the prompt pulse. In order to construct off-line spectra for several sets of time windows, an event by event data acquisition system was developed. For each delayed photon, not only the Doppler velocity of the reference sample was registered but also the time delay with respect to the previous prompt pulse. The digital time signal was obtained by using a time-to-amplitude convertor (TAC) followed by an analog-to-digital convertor (ADC). The start of the TAC was given by the detection of the photon and the stop by a periodic signal (period T_B) that coincides with the detection of the prompt pulse. A schematic overview of the electronics is given in Fig. 6. In our experiment the data of photons with a delay between 2.64 ns and 21.12 ns were stored in 47 time channels.

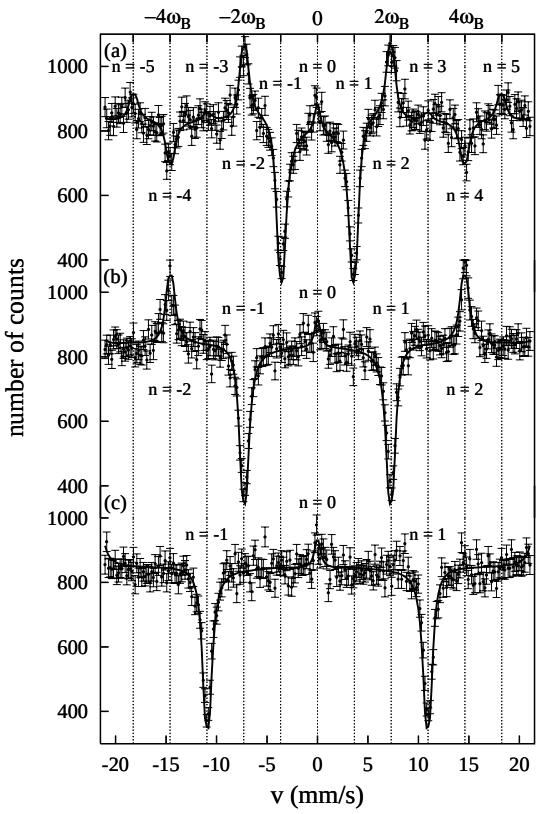

FIG. 7: Spectra obtained with stroboscopic detection for two single-line absorbers ($K_4Fe(CN)_6.3H_2O$) for three sets of time windows with different period T. All time windows are symmetric around T/2 and have an allowed fraction $F = 0.35$. (a) $T = 23.6$ ns. (b) $T = 11.8$ ns. (c) $T = 7.9$ ns.

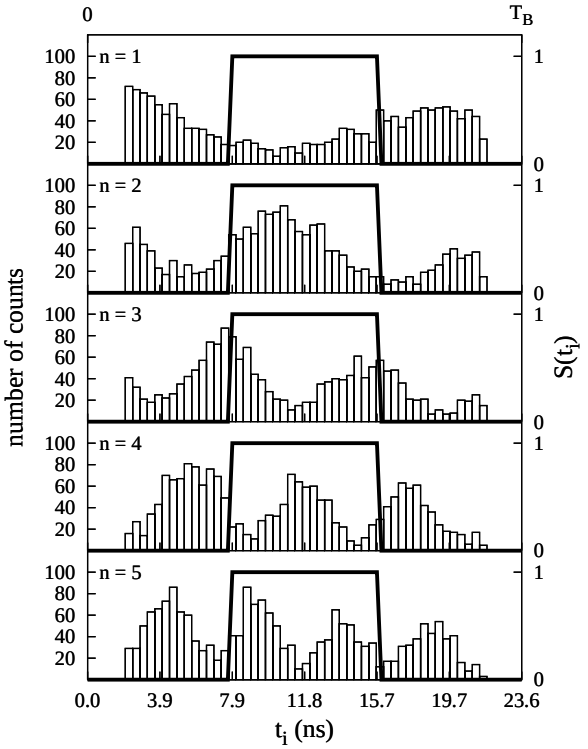

FIG. 8: Time spectra at the position of the stroboscopic resonances of order n of Fig. 7(a) ($v_n = n \times 3.65$ mm/s). The solid line indicates the time window ($S(t)$) used to construct the velocity spectrum in Fig. 7(a).

V. EXPERIMENTAL RESULTS AND DISCUSSION

All experimental spectra that are discussed in this section are constructed using the same data set. The only difference is the selected set of time windows. Therefore, the series of spectra that will be shown are ideal to demonstrate the theory presented above and to discuss the influence of the time-window frequency and the time-window symmetry on the stroboscopic spectra. In a first example, a square time window with a frequency, ω_T, equal to the bunch frequency, ω_B, was selected. The time window was chosen symmetric around the center between two bunches and the allowed fraction was fixed to $F = 0.35$. The number of photons accumulated within this time window as a function of the Doppler velocity is shown in Fig. 7(a). We can clearly distinguish several equally spaced resonances. Figure 8 shows the experimental time spectra for the fixed velocities, v_n, corresponding to the position of the resonances. The time window that was used to construct the velocity spectrum is indicated by the solid line. It can be clearly seen that the quantum-beat frequency is a multiple of the time-window frequency and, hence, the resonances in spectrum 7(a) can be identified as the stroboscopic resonances. Because both samples are made of the same compound, the resonance condition is given by $\Delta = n\omega_T$. From this relation the position of the resonances can be calculated to be $v_n = n(\omega_T/\omega_r)c = n \times 3.65$ mm/s and the velocity scale can be calibrated. The sign of the resonances can also be deduced by looking at the time spectra of Fig. 8. For $n = 1$ the time window selects a minimum in the intensity, which is in agreement with the negative resonance at 3.65 mm/s in velocity spectrum of Fig. 7(a). For $n = 2$ a maximum is selected, resulting in a positive resonance at 7.3 mm/s. Similar deductions can be made for the higher order resonances. A more quantitative discussion is based on the calculation of the coefficients s_n. This can be done analytically using Eq. 26 with $\exp(-in\omega_T t_0) = (-1)^n$ and $F = 0.35$ (table I). Because the selected time windows are symmetric around $T/2$, s_n is real for all n. Hence, only lorentzian-like resonances are found. Positive s_n correspond to positive resonances, negative s_n to negative resonances. From the relation $s_{-n} = s_n^* = s_n$ it is clear that the stroboscopic resonances of order n and $-n$ must be identical. Note that the signal-to-baseline ratio of the different resonances is proportional to $|s_n|$ for $n \neq 0$. For the central resonance the signal-to-baseline ratio is reduced due to the radiative

n	s_n
0	0.35
1	-0.284
2	0.129
3	0.017
4	-0.076
5	0.045

TABLE I: Coefficients s_n for square time windows symmetric around $T/2$ and with an allowed fraction $F = 0.35$.

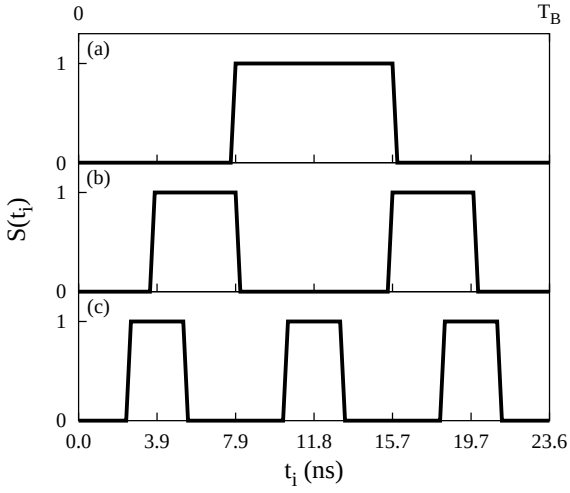

FIG. 9: Different sets of time windows ($S(t)$) with different period T used for the spectra in Fig. 7. All time windows are symmetric around T/2 and have an allowed fraction $F = 0.35$. (a) $T = 23.6$ ns. (b) $T = 11.8$ ns. (c) $T = 7.9$ ns.

coupling between the samples.

In section III.C it was deduced that the shift of the stroboscopic resonances is linear with the time-window frequency, ω_T. The higher the frequency or, equivalently, the smaller the period of the set of time windows, the larger the distance between two different stroboscopic order resonances. The spectrum in Fig. 7(b) was obtained by doubling the time-window frequency ($\omega_T = 2\omega_B$, see Fig. 9(b)). As a consequence, the shift of the stroboscopic resonances with respect to the central resonance has also doubled ($v_{2n} = 2n \times 3.65$ mm/s). In Fig. 7(c), the spectrum for a set of time windows with three times the bunch frequency ($\omega_T = 3\omega_B$, see Fig. 9(c)) is given. For this set of time windows, the first-order stroboscopic resonance is positioned at 3×3.65 mm/s $= 10.95$ mm/s. Remark that all three sets of time windows are chosen so that they have the same symmetry and allowed fraction. Therefore, the associated coefficients s_n are equal. This explains why the stroboscopic resonances of the same order have the same shape and signal-to-baseline ratio.

Until now, the time windows were chosen symmetric around $t_0 = T/2$, resulting in lorentzian-like resonances.

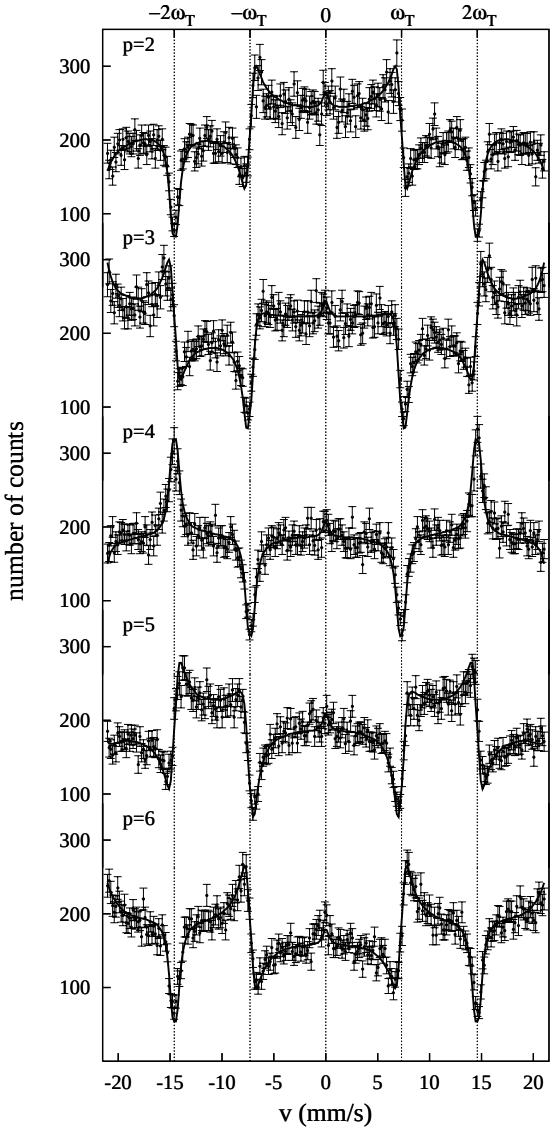

FIG. 10: Spectra obtained with stroboscopic detection for two single-line absorbers ($K_4Fe(CN)_6.3H_2O$) for five sets of time windows with the same period $T = 11.8$ ns and allowed fraction $F = 1/12$. The time windows are symmetric around $pT/8$.

In section III.D we found that the shape of the resonances is changed by adapting the phase of the coefficients s_n. For symmetric time windows this phase is determined by the center of the time window. For the spectra in Fig. 10, five different time windows with a period of 11.8 ns and an allowed fraction $F = 1/12$ were shifted in time (Fig. 11). The center of the time window was fixed to $pT/8$ with $p = 2, ..., 6$. Hence, Eq. 26 reduces to

$$s_n = \exp(-inp\frac{\pi}{4})\frac{\sin(n\pi F)}{n\pi}. \qquad (31)$$

The values of the real scaling factors $\sin(n\pi F)/(n\pi)$ for

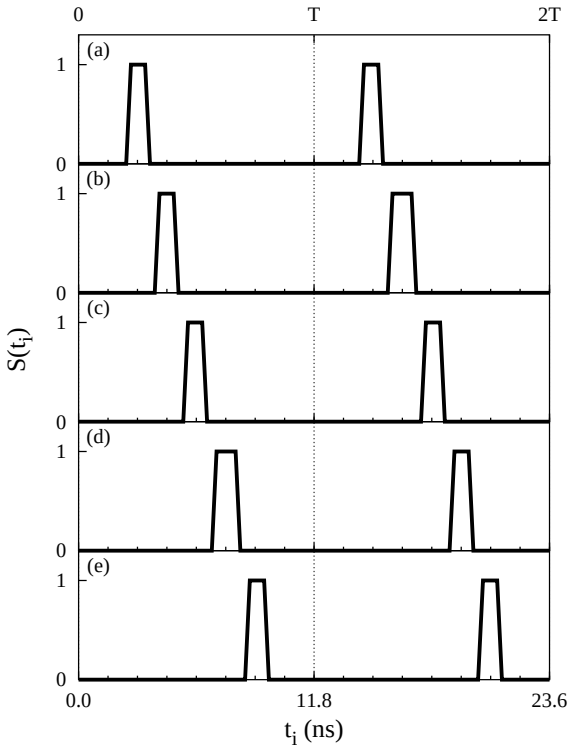

FIG. 11: Set of time windows ($S(t)$) with a period $T = 11.8$ ns used for the spectra in Fig. 10. All time windows have an allowed fraction $F = 1/12$ and are symmetric around $pT/8$.

n	$sin(n\pi F)/(\pi F)$
0	0.0833
1	0.0824
2	0.0796

TABLE II: $sin(n\pi F)/(\pi F)$ for $F = 1/12$.

$F = 1/12$ are tabulated in table II. The additional phase phase factor is given by $\exp(-inp\pi/4)$. For $p = 2$ s_1 is imaginary and, therefore, a dispersion-like resonance is found at 7.3 mm/s in the first spectrum of Fig. 10. Because of the relation $s_{-1} = s_1^* = -s_1$, an identical resonance reflected around the baseline is found at -7.3 mm/s. For the same time window, $s_{-2} = s_2$ is real and negative, resulting in identical negative lorentzian-like resonances at -14.6 mm/s and 14.6 mm/s. By shifting the set of time windows, the phase of the coefficients s_n is also shifted. This is illustrated in Fig. 12. Note that for s_2 the phase shifts two times faster as for s_1. In Fig. 10 the shape of the resonances accordingly changes. In the next section we will show that shifting the set of time windows is equivalent to tilting the phase shifter in an interferometer experiment.

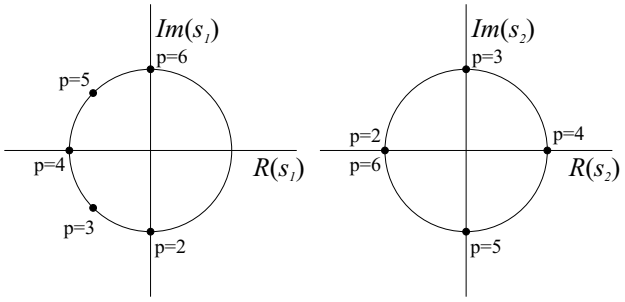

FIG. 12: Phase of the coefficients s_1 and s_2 for time windows with the same allowed fraction and a different center $pT/8$.

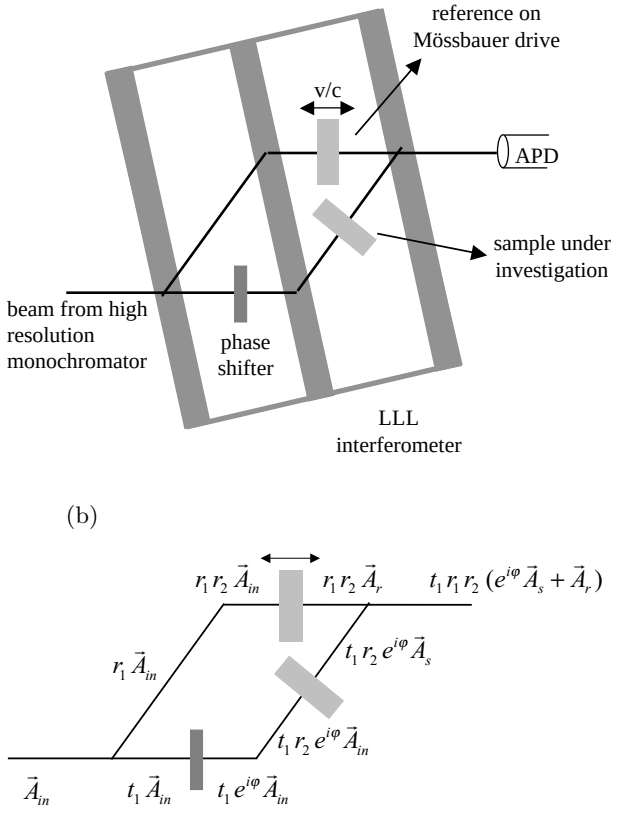

FIG. 13: (a) Scheme with both samples in the different paths of an LLL-type interferometer. (b) The amplitude at different positions in the scheme.

VI. STROBOSCOPY AS INTERFEROMETRY

From the previous sections it is clear that a stroboscopic detection experiment can be designed so that nice energy-resolved spectra are obtained. Important thereby is that the time-window frequency should be chosen larger than the resonant frequency range in the samples. An interesting feature is the lack of radiative coupling at the velocities corresponding to the higher order stroboscopic resonances. Therefore, the stroboscopic de-

process	new amplitude	
	first path	second path
transmission through / reflection by the first crystal	$t_1\vec{A}_{in}$	$r_1\vec{A}_{in}$
transmission through the phase shifter	$t_1 e^{i\phi}\vec{A}_{in}$	
reflection by the second crystal	$t_1 r_2 e^{i\phi}\vec{A}_{in}$	$r_1 r_2\vec{A}_{in}$
transmission through the sample	$t_1 r_2 e^{i\phi}\vec{A}_s$	$r_1 r_2\vec{A}_r$
reflection by / transmission through the third crystal (identical to the first crystal)	$t_1 r_1 r_2 e^{i\phi}\vec{A}_s + t_1 r_1 r_2\vec{A}_r$	

TABLE III: The amplitude for both paths in the interferometer.

tection scheme can be an alternative for a time-integrated measurement in a detection scheme with both samples placed in the different paths of an LLL-type interferometer[15,16] (Fig. 13(a)). An LLL-type interferometer consist of three blades of one crystal. At the first blade the beam is split in two spatially separated paths. The second blade reflects the beam so that both paths rejoin at the position of the third blade. The typical construction of the interferometer has two important consequences. First, because both paths inside the interferometer are separated in space there is no radiative coupling between the samples placed inside the different paths. Second, both scattering paths are coherent. Therefore, one delocalized photon has a probability amplitude to excite the nuclei in both samples. If we assume a visibility of 100%, the total scattering amplitude is the sum of the amplitudes for both scattering paths (Fig. 13(b), table III)

$$\begin{aligned}\vec{A}(\omega,\Delta) &= t_1 r_1 r_2(e^{i\phi}\vec{A}_s + \vec{A}_r)\\ &= t_1 r_1 r_2[e^{i\phi} f_s(\omega-\omega_i) + f_r(\omega-\omega_r-\Delta)]\vec{A}_{in}.\end{aligned} \tag{32}$$

with r_1, t_1 and r_2 the reflection and transmission coefficients of the crystals of the interferometer. The factor $e^{i\phi}$ is the phase factor induced by the phase shifter in the path of the sample under investigation. The time-integrated intensity can be calculated using the square of the amplitude

$$I(\Delta) = \int_{-\infty}^{+\infty} dt\ |\vec{A}(t,\Delta)|^2. \tag{33}$$

Using Parseval's theorem and replacing the amplitude by Eq. 32 we find

$$\begin{aligned}I(\Delta) &= \frac{1}{2\pi}\int_{-\infty}^{+\infty} d\omega\ |\vec{A}(\omega,\Delta)|^2\\ &\sim \frac{1}{2\pi}\int_{-\infty}^{+\infty} d\omega\ \left\{|f_s(\omega-\omega_i)\vec{A}_{in}|^2 + |f_r(\omega-\omega_r)\vec{A}_{in}|^2 + 2\Re\left[e^{i\phi}[f_s(\omega-\omega_i)\vec{A}_{in}]\cdot[f_r(\omega-\omega_r-\Delta)\vec{A}_{in}]\right]\right\}\\ &\sim \beta_{s,0}+\beta_{r,0}+2\Re(e^{i\phi}\alpha_0(\Delta))\end{aligned} \tag{34}$$

The spectrum contains a baseline ($\sim(\beta_{s,0}+\beta_{r,0})$) with superposed resonances described by

$$2\Re(e^{i\phi}\alpha_0(\Delta)). \tag{35}$$

Let us compare this formula with Eq. 30 which describes the stroboscopic resonances of order $n \neq 0$ for ω_T larger than the frequency range in the sample. For a time window symmetric around t_0, s_n can be replaced by Eq. 25. Hence, in this case, equation 30 can be written as

$$I^n_{int}(\Delta) = s'_n\ 2\Re[\exp(-in\omega_T t_0)\ \alpha_n(\Delta)] \tag{36}$$

with s'_n a real scaling factor defined by Eq. 24. The similarity between Eq. 35 and Eq. 36 is clear. Both equations describe resonances with an identical shape. The only difference is the origin of the phase factor. In an interferometer experiment, the phase factor $\exp(i\phi)$ can be changed by tilting the phase shifter, while in a stroboscopic measurement, the phase factor $\exp(-in\omega_T t_0)$ can be adapted by shifting the time window. From this equivalence it is clear that, similar as in an interferometer experiment[17] the phase information can be extracted.[18] Although both detection schemes produce comparable spectra, the corresponding experimental setup is completely different. Thereby, the simplicity of the heterodyne setup presented in Fig. 1 can be advantageous.

VII. COMPARISON BETWEEN STROBOSCOPIC DETECTION AND OTHER MÖSSBAUER TECHNIQUES

Radioactive Source	Synchrotron Radiation
restricted to isotopes for which a good source is available	can be tuned over a wide energy range (up to $\sim$ 100 keV)
narrow energy bandwidth	broad energy bandwidth
radiation over 4π	small beam size low angular divergence high intensity
unpolarized light	polarized light
background due to non-scattered photons	non-scattered photons can be gated in time resulting in a large signal-to-baseline ratio
relatively cheap experiment can be performed in local laboratory	restricted beam time at large scale facility

TABLE IV: Comparison of a radioactive source and the synchrotron source in a Mössbauer experiment.

So far, the principles of stroboscopic detection of nuclear resonant forward-scattered synchrotron radiation have been extensively discussed. In this section we focus on the strengths and weaknesses of the technique. Stroboscopic detection of nuclear forward-scattered radiation is a technique based on the Mössbauer effect that uses the synchrotron as a source of radiation. The production mechanisms of synchrotron radiation and the radiation produced by a radioactive source are totally different. Therefore, both sources have totally different properties (table IV). In a radioactive source, almost monochrome radiation is produced by gamma decay. As a consequence, for each isotope another source is needed. Synchrotron light, on the other hand, is produced by relativistic electrons bent by a magnet or a series of magnets, e.g. an undulator. An undulator can be tuned to produce radiation with an energy in a range from $1 \sim 100$ keV. Hence, the synchrotron source can be used for resonant scattering by a wide range of Mössbauer isotopes. A second advantage of the synchrotron source is the high intensity and the good collimation of the beam. This is favorable for grazing incidence experiments[19] and for the study of small samples, e.g., a sample embedded in a diamond anvil cell[7,20]. Moreover, in a nuclear resonant scattering experiment with synchrotron radiation, the non-scattered photons are prompt. Therefore, time gates can be chosen such that the spectra contain only data from photons that have interacted with the samples, resulting in a signal-to-baseline ratio that is generally larger than in a conventional Mössbauer spectrum. Another important difference between both sources is the polarization. The selection rules applied in the case of linear polarized synchrotron light gives rise to other allowed transitions[8] than in the case of the unpolarized light of a radioactive source. Therefore, Mössbauer spectroscopy with a radioactive source and nuclear resonant scattering of synchrotron radiation are complementary techniques. The most important restriction of the synchrotron source is that the beam can only be provided by a large scale facility. As a consequence, only a limited period of beam time is available.

In table V different synchrotron Mössbauer techniques are compared. A big advantage of stroboscopic detection is that energy-resolved spectra can be produced without the restriction that the sample under investigation has to be mounted on a special device such as a Mössbauer drive or a rotor. Therefore, samples embedded in, e.g., a diamond anvil cell[7] or mounted in a cryostat can easily be studied. Another advantage of stroboscopic detection is that phase information can be obtained by shifting the time window. The restrictions of the technique are related to the time resolution of the detector and the electronics. From the previous sections it is clear that the stroboscopic spectra are easier to analyze if the time-window frequency is of the order of the range of the resonance frequencies in the sample. Up till now typical time-window frequencies that can be reached with an Avalanche Photo Diode (APD) detector[21] were lower than 8×10^8 Hz. In order to reach high frequencies, detectors with a good time resolution are needed. Unfortunately, such detectors are generally less efficient. For the study of narrow band spectra, which are generally found in the case of long-lived isomers, lower time-window frequencies are convenient. Therefore, in this case, the restriction on the time resolution is not so severe. The restriction on the bunch mode is also associated with the detector resolution. The faster the time window can start after the prompt pulse, the higher the time-window frequency and, consequently, the bunch frequency can be.

VIII. CONCLUSION

In conclusion, we discussed the principles of stroboscopic detection of nuclear forward-scattered synchrotron radiation and compared this technique with other Mössbauer techniques. It was pointed out how a stroboscopic experiment must be designed in order to obtain nice energy-resolved spectra. We showed that the total spectrum is a superposition of different stroboscopic order spectra. From the position of the resonances within one stroboscopic order the hyperfine parameters can be deduced, similar to conventional Mössbauer spectroscopy. The distance between the stroboscopic order

spectra is linearly connected to the time-window frequency. Therefore, in order to obtain spectra for which different stroboscopic order spectra do not overlap, the time-window frequency should be larger than the range of resonance frequencies in the sample. If the latter condition on the time windows is technically infeasible, the interpretation of the spectra becomes less straightforward. However, these spectra can still be analyzed in terms of hyperfine parameters. The shape of the resonances depends on the symmetry of the time window. A time window being symmetric around the center between two bunches gives rise to lorentzian-like resonances. Shifting the time window in time gives rise to dispersion-like curves or resonances with a combination of a lorentzian-like and dispersion-like shape. It was shown that shifting the time window is equivalent to tilting a phase shifter in an interferometer experiment. From the comparison between different Mössbauer techniques, it is clear that the unique features of stroboscopic detection make this technique complementary to and in some cases advantageous over other techniques.

Acknowledgments

The authors would like to thank C. L'abbé for the stimulating discussions. This work was supported by Research Programmes of the Fund for Scientific Research - Flanders, Belgium and the Interuniversitary Institute for Nuclear Sciences (IINS - Belgium). This work was also supported by the IUAP programme P4-07 financed by the Belgian Federal Office for Scientific, Technical and Cultural Affairs and a Grant-in-Aid for COE Research(10CE2004) from the Ministry of Education, Culture, Sports, Science and Technology of Japan. R. Ca. and K. V. are very grateful to the Fund for Scientific Research Flanders (Belgium) for financial support. J. L. would like to thank the Interuniversitary Institute for Nuclear Sciences (Belgium) for financial support. The experiments were performed at SPring-8 (experiment 2001A0088-CMD-np).

* Electronic address: riet.callens@fys.kuleuven.ac.be

[1] S. Ruby, J.Phys. (Paris) Colloq. **35**,C6-209 (1974).
[2] E. Gerdau, R. Rüffer, H. Winkler, W. Tolksdorf, C. P. Klages, and J. P. Hannon, Phys. Rev. Lett. **54**, 835 (1985).
[3] J. B. Hastings, D. P. Siddons, U. van Bürck, R. Hollatz, ans U. Bergmann, Phys. Rev. Lett. **66**,770 (1991).
[4] for an overview see: *Nuclear Resonant Scattering of Synchrotron Radiation (Part A)*, edited by E. Gerdau and H. de Waard [Hyperfine Interact. **123/124** (1999)] and references therein.
[5] R. Röhlsberger, T. S. Toellner, W. Sturhahn, K. W. Quast, E. E. Alp, A. Bernhard, E. Burkel, O. Leupold, and E. Gerdau, Phys. Rev. Lett. **84**, 1007 (2000); R. Röhlsberger, K. W. Quast, T. S. Toellner, P. L. Lee, W. Sturhahn, E. E. Alp, and E. Burkel, Phys. Rev. Lett. **87**, 47601 (2001).
[6] G. V. Smirnov U. van Bürck, A. I. Chumakov, A. Q. R. Baron, and R. Rüffer, Phys. Rev. B **55**, 5811 (1997).
[7] R. Callens, R. Coussement, C. L'abbé, S. Nasu, K. Vyvey, T. Yamada, Y. Yoda, and J. Odeurs, Phys. Rev. B **65**, 180404(R) (2002).
[8] G. V. Smirnov, Hyperfine Interact. **123-124**, 31 (1999).
[9] R. Coussement, S. Cottenier, C. L'abbé, Phys. Rev. B **54**, 160 03 (1996).
[10] R. Coussement, J. Odeurs, C. L'abbé and G. Neyens, Hyperfine Interact. **125**, 113 (2000); C. L'abbé, R. Callens, and J. Odeurs, Hyperfine Interact. **135**, 275-294 (2001).
[11] C. L'abbé, R. Coussement, J. Odeurs, E. E. Alp, W. Sturhahn, T. S. Toellner, and C. Johnson, Phys. Rev. B **61**, 4181 (2000).
[12] J. Z. Tischler, B. C. Larson, L. A. Boatner,E. E. Alp, and T. Mooney, J. Appl. Phys. **79**, 3686 (1996).
[13] Y. Yoda, M. Yabashi, K. Izumi, X. W. Zhang, S. Kishimoto, S. Kitao, M. Seto, T. Mitsui, T. Harami, Y. Imai, S. Kikuta, Nucl. Instrum. Methods A **467**, 715 (2001).
[14] W. Kerler, Zeitschrift für Physik **167**, 194-204 (1962).
[15] Y. Hasegawa, Y. Yoda, K. Izumi, T. Ishikawa, S. Kikuta, X. W. Zhang, and M. Ando, Phys. Rev. B **50**, 17748 (1994).
[16] K. Izumi, Y. Yoda, T. Ishikawa, X. W. Zhang,M. Ando, and S. Kikuta, Jpn. J. Appl. Phys. **34**, 4258 (1995).
[17] W. Sturhahn, Phys. Rev. B **63**, 094105 (2001).
[18] R. Callens et al., to be published.
[19] D. L. Nagy, L. Bottyan, L. Deak, E. Szilagyi,H. Spiering,J. Dekoster, and G. Langouche, Hyperfine Interact. **126**, 353 (2000) and references therein.
[20] R. Lübbers, G. Wortmann, H. F. Grünsteudel, Hyperfine Interact. **123/124**, 529 (1999).
[21] A. Q. R. Baron, Hyperfine Interact. **125** 29 (2000).

Time Differential nuclear resonant forward scattering	Stroboscopic Detection	Synchrotron Mössbauer Source[6]	Nuclear Lighthouse Effect[5]
time differential spectra	energy-resolved spectra	energy resolved spectra	angular spectra equivalent with time differential spectra (very good resolution)
sample under investigation stands freely	sample under investigation stands freely	sample under investigation is mounted on a Mössbauer drive	sample under investigation is mounted on a rotor
phase information can be obtained by including an interferometer in the setup	phase information can be obtained by shifting the time window	no phase information	no phase information
applicable on a wide range of isotopes	applicable on a wide range of isotopes	up till now only applicable on ^{57}Fe-samples	applicable on a wide range of isotopes
ideal bunch interval is of the order of the life time of the isomer	ideal time-window frequency is of the order of the resonance frequency range in the sample		
	favorable for long-lived isomers (narrow bandwidth)		favorable for short-lived isomers (because of the good time resolution)
bunch interval must be in the order of the life time of the isomer	bunch interval must be long enough in order to cut the prompt pulse	no bunch mode requirements	no bunch mode requirements

TABLE V: Comparison between time-differential nuclear resonant forward scattering, stroboscopic detection of of nuclear resonant forward-scattered radiation, the Synchrotron Mössbauer Source and the Nuclear Lighthouse Effect.